

Rheocoalescence: Relaxation time through coalescence of droplets

Sarath Chandra Varma,[†] Abhineet Singh Rajput,[†] and Alope Kumar^{*,†}

Department of Mechanical Engineering, Indian Institute of Science, Bangalore, India

E-mail: *alokekumar@iisc.ac.in

Abstract

Dynamics of the pendant drop coalescing with a sessile drop to form a single daughter droplet is known to form a bridge. The bridge evolution begins with a point contact between the two drops leading to a liquid neck of size comparable to the diameter of the drops. To probe this phenomenon in polymeric fluids, we quantify the neck radius growth during coalescence using high speed imaging. In the current study, we unveil the existence of three regimes on basis of concentration ratio c/c^* namely, inertio-elastic $c/c^* < c_e/c^*$, viscoelastic $c_e/c^* < c/c^* < 20$ and elasticity dominated regimes $c/c^* > 20$. Our results suggest that the neck radius growth with time (t) obeys a power-law behaviour t^b , such that the coefficient b has a steady value in inertio-elastic and viscoelastic regimes, with a monotonic decrease in elasticity dominated regime. Based on this dependence of b on concentration ratios, we propose a new measurement technique Rheocoalescence to obtain the relaxation time of these fluids. We also show a deviation from universality proposed in literature for the elasticity dominated regime.

Introduction

Coalescence is a singular event in which two or more drops merge to form a single daughter droplet.¹ The dynamics of this singular event is governed by the liquid bridge formation and its growth. This temporal growth bears the signature of the underlying governing equation.² Such natural processes are observed in raindrop condensation^{3,4} and industrial processes such as paint spray coatings,^{5,6} combustion process,⁷ droplets on surfaces,⁸ and processes linked to life.^{9,10} Depending on the relative orientation of droplets, the phenomenon can occur in physically different configurations, i.e., pendant-pendant,^{11–13} sessile-pendant,¹⁴ and sessile-sessile.^{15–17} The entire evolution process in pendant-pendant and sessile-pendant configurations is driven by a balance between surface tension, viscous and inertial effects, and Laplace pressure.^{2,13} In Newtonian fluids, based on the force balance the evolution lies either in the inertial dominated¹⁸ or viscous dominated regime.^{11,12} Apart from these regimes, a new regime of inertially limited viscous regime¹⁹ was proposed in Newtonian droplet coalescence, wherein all inertial, viscous, and surface tension forces are essential.

The kinematics of the coalescence phenomenon in pendant-pendant and sessile-pendant configurations is characterized by the temporal evolution of the liquid bridge of neck radius R and bridge semi-width H . In Newtonian droplets, the temporal evolution of neck¹² was demonstrated to follow the scale of $R \sim t^b$, where, R is the neck radius and t is time. Based on viscosity of the fluid, the dynamics of the neck radius evolution has been identified to have dominant viscous regime at early times and inertial regime at later instances. In the viscous regime,¹² the neck radius has a scaling of $R \sim t$. Similarly in the inertial regime,^{12,18} neck radius has a scale of $R \sim t^{0.5}$. In literature, regime-wise universality^{2,11–13,18,20–32} is elucidated both experimentally and analytically. In the viscous regime,¹⁸ the neck radius has a universal scaling of $R^* \sim (t^*)$, in which $R_c = R_o$ and $t_c = \eta R_o / \sigma$, where R_o is radius of the drop, η is viscosity and σ is surface tension. Similarly, in the inertial regime^{2,18} neck radius has a universal scale of $R^* \sim (t^*)^{0.5}$, in which $R_c = R_o$ and $t_c = \sqrt{\rho R_o^3 / \sigma}$, ρ being density.

The paradigm of a coalescence phenomenon in rheologically complex fluids is significantly more involved. Polymeric fluids are a distinct subgroup of complex fluids that exhibit strong non-Newtonian characteristics due to molecular chain interactions or relaxations. Relaxation time (λ) is the fingerprint of elasticity and molecular relaxations. A recent study on aqueous solutions of polymer droplets on both pendant-sessile¹⁴ and sessile-sessile¹⁵ configurations emphasized the role of relaxation time on the dynamics of neck radius evolution. The former study on pendant-sessile¹⁴ configuration showed that for $Wi \sim \mathcal{O}(1)$, where $Wi = \lambda U/R$ (λ is relaxation time, U is neck velocity) is Weissenberg number, the neck radius growth follows the scale of $R \sim t^{0.36}$. The study also showed that for $Wi \sim \mathcal{O}(10^{-3} - 10^{-4})$, the neck radius growth follows the scale of $R \sim t^{0.39}$. The study also showed the universality in the coalescence of polymeric droplets by non-dimensionalising the neck radius and time with $R_c = \sqrt{\nu_o \lambda}$ and $t_c = \text{Oh} \lambda (c/c^*)^{1.2}$, respectively, where, ν_o is the kinematic viscosity of the fluid, λ is relaxation time, Oh is Ohnesorge number and c/c^* is concentration ratio, has the universal scaling of $R^* \sim t^{0.36}$. Similar to the relaxation time, concentration ratio c/c^* is another important parameter representing the chain entanglements. Previous studies on coalescence of polymeric droplets were done on the solutions of $c/c^* < 10$.¹⁴ In the present study we investigate the coalescence of the polymeric droplets with $c/c^* > 10$.

Despite of many applications of coalescence of polymeric droplets in microfluidics and interfacial rheology,^{33,34} this phenomenon is sparsely studied. In the present study, we demonstrate that the coalescence of sessile and hanging pendant drops of aqueous polymer solutions have different regimes, along with the dependence of neck growth on relaxation time. To experimentally depict the effect of relaxation time on neck growth, we study the coalescence of droplets for various concentrations of polyethylene oxide (PEO) of molecular weights $M_w = 5 \times 10^6$ g/mol and $M_w = 4 \times 10^6$ g/mol. Experimental observation of neck radius growth of various concentrations is demonstrated by scaling analysis based on linear Phan-Thein-Tanner (PTT)^{35,36} constitutive equation. Our results contrast the universal behaviour proposed previously and hold enormous promise for opening a new method to determine the

relaxation time of the fluid.

Materials and methods

Polyethylene oxide (PEO) of different molecular weights M_w are added to DI water in sufficient quantities to get the various concentrations c . All the solutions are stirred at 300 RPM for different durations. Polymers used in the present study along with their molecular weights are listed in Table-I. Concentrations of the polymers are chosen in a way that the solution types vary in a range of semi-dilute unentangled, and semi-dilute entangled regimes. Regimes of semi-dilute unentangled, and semi-dilute entangled are differentiated using the critical concentration c^* and the entanglement concentration c_e respectively. The critical concentration of PEO for different molecular weights is obtained from the $[\eta]$ intrinsic viscosity using the Flory relation $c^* = 1/[\eta]$ alongside the Mark-Houwink-Sakurada correlation³⁷ $[\eta] = 0.072M_w^{0.65}$ and the entanglement concentration c_e is obtained using the relation $c_e \approx 6c^*$.³⁸ The values of c^* and c_e are listed in Table-I. All the concentrations used in present study along with their concentration ratios c/c^* are given in Table-II.

Table 1: List of molecular weights of polymers along with their critical and entanglement concentrations.

Polymer	M_w (g/mol)	c^* (% w/v)	c_e (% w/v)
PEO	5×10^6	0.061	0.366
PEO	4×10^6	0.071	0.426

Experiments are performed on a Polydimethylsiloxane (PDMS) coated glass substrate. Before the experiments the substrate are cleaned with detergent followed by sonication with acetone and DI Water respectively for 20 mins each. The substrates are then dried in a hot air oven 95°C for 30 mins. PDMS is prepared by adding the curing agent (Syl Gard 184 Silicone Elastomer Kit, Dow Corning) to PDMS in the ratio of 1:10. This mixture is agitated and kept for desiccation for 30 minutes until all visible gas bubbles are removed. Glass substrates are coated with PDMS using a spin coater at 5000 rpm for 60 s. The coated

substrate are cured by keeping them in a hot air oven at 90°C for at least 90 min. Surface tension σ of the solutions are measured by pendant drop method using optical contact angle measuring and contour analysis system (OCA25) instrument from Dataphysics. All the solutions were found to have surface tension values of 0.062 ± 0.02 N/m. We have assumed the density of all the solutions to be 1000 kg/m³.

Table 2: Rheological properties of the solutions. (Note: Relaxation time values given in blue are obtained from the correlations, remaining values are obtained from the crossover of G' and G'').

M_w (g/mol)	c (% w/v)	c/c^* (% w/v)	η_o (Pa.s)	λ (s)
5×10^6	0.1	1.64	0.006	0.0017
	0.2	3.28	0.018	0.0025
	0.4	6.56	0.06	0.064
	0.75	12.29	0.8	0.165
	1	16.39	4.5	0.5
	1.5	24.59	20	0.67
	1.75	28.68	40	1.325
	2.25	36.88	72	1.43
	2.5	40.98	85	1.59
	2.75	45.08	190	2.0
	3	49.18	210	2.25
4×10^6	3.25	53.28	230	2.5
	0.5	8.19	0.038	0.058
	1.0	16.39	0.6	0.25
	1.5	24.59	2	0.57
	2.0	32.79	10	1.04
	2.5	40.98	16	1.65
	3.0	49.18	75	2.4

Rheology

Rheometry

Rheology experiments are performed on Anton Paar[®] MCR 302 rheometer using a cone and plate 40 mm, 1° geometry to characterize the viscoelastic behaviour of the solutions. The viscosity variation with shear rate for the chosen solutions is shown in Fig. 1(a). All

the concentrations have shown the shear thinning behavior. The zero shear viscosity of the solutions is obtained by fitting the viscosity data in the form of Carreau-Yasuda model³⁹ represented by equation $\eta - \eta_\infty = (\eta_o - \eta_\infty) [1 + (\Gamma\dot{\gamma})^p]^{\frac{n-1}{p}}$, where η_o , η_∞ , $\dot{\gamma}$, n , Γ and p represent zero-shear viscosity, infinite-shear viscosity, shear rate, flow behavior index, time constant and width of the transition region between η_o and the power-law region respectively. The values of η_o for all the concentrations are listed in Table-II. Viscoelasticity of the polymer solutions is characterized by performing the small amplitude oscillatory shear SAOS experiments in rheometer. The variation of storage modulus G' and loss modulus G'' with frequency ω is shown in Fig. 1(b) for 1% w/v, 1.5% w/v, 2.25% w/v, 2.75% w/v and 3.25% w/v concentrations as a representation.

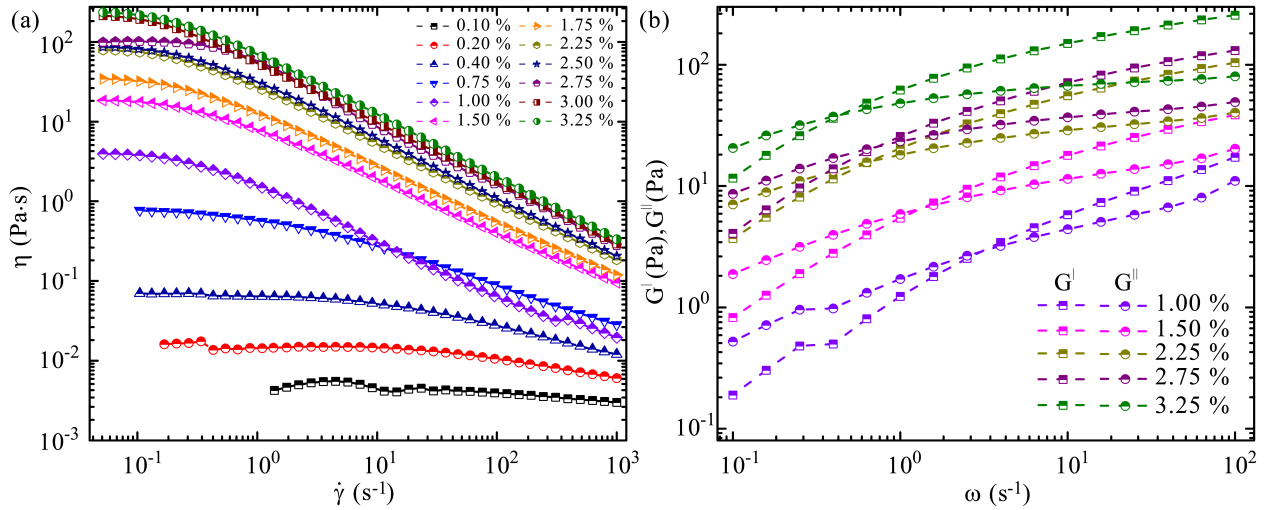


Figure 1: Rheological behavior of PEO $M_w = 5 \times 10^6$ g/mol (a) Dependence of viscosity on shear rate for different concentrations. (b) Variation of the storage modulus G' and the loss modulus G'' with frequency obtained from SAOS experiments for 1% w/v, 1.5% w/v, 2.25% w/v, 2.75% w/v and 3.25% w/v concentrations. (Standard deviation of the data is less than 2% for all the concentrations)

Relaxation time

In SAOS, relaxation time λ of the polymer solutions is defined as $\lambda = 1/\omega_c$, where ω_c is the crossover frequency for the G' and G'' curves. It is observed that for concentrations $c > 1\%$

w/v, SAOS has a crossover. But, for $c < 1\%$ w/v, there is no crossover as rheometer has the maximum frequency of 100 s^{-1} which corresponds to time scale of 10^{-2} s . So, for $c < 1\%$ w/v, the relaxation times are estimated using the Zimm model.³⁹

$$\lambda_z = \frac{1}{\zeta(3\nu)} \frac{[\eta]M_w\eta_s}{N_A k_B T} \quad (1)$$

where, η_s is the solvent viscosity, k_B is the Boltzmann constant, λ_z is the Zimm relaxation time, T is the absolute temperature and ν is fractal polymer dimension determined using the relation $a = 3\nu - 1$, where a is the exponent of Mark-Houwink-Sakurada correlation. For the solutions in semi-dilute unentangled λ_{SUE} and semi-dilute entangled λ_{SE} regimes, the relaxation times are calculated using these correlations : $\lambda_{\text{SUE}} = \lambda_z \left(\frac{c}{c^*}\right)^{\frac{2-3\nu}{3\nu-1}}$ and $\lambda_{\text{SE}} = \lambda_z \left(\frac{c}{c^*}\right)^{\frac{3-3\nu}{3\nu-1}}$ ⁴⁰⁻⁴² respectively. The relaxation times for the chosen concentrations are listed in Table-II. The relaxation times obtained for $c > 1\%$ w/v from the crossover frequency of G' and G'' are in good agreement with Zimm model estimated values. As a representation the relaxation time obtained from the frequency sweep for 1.5% w/v is 0.67 s , compared with the value obtained from the Zimm model as 1 s .

Experiments

A drop of diameter $2.25 \pm 0.1 \text{ mm}$ is dispensed on a substrate. To achieve coalescence a pendant drop of the same diameter is brought towards the dispensed drop with 10^{-4} approach velocity to ensure the controlled coalescence. Experiments are conducted at a temperature of 25°C and 1 atm pressure. Fig. 2(a) shows the schematic of the experimental setup. The coalescence process is captured at 170000 fps using a Photron Fastcam mini high-speed camera with a Navitar lens attachment. The drops are illuminated using an LED light source. Data extraction from the images is performed using custom-written algorithms in MATLAB.

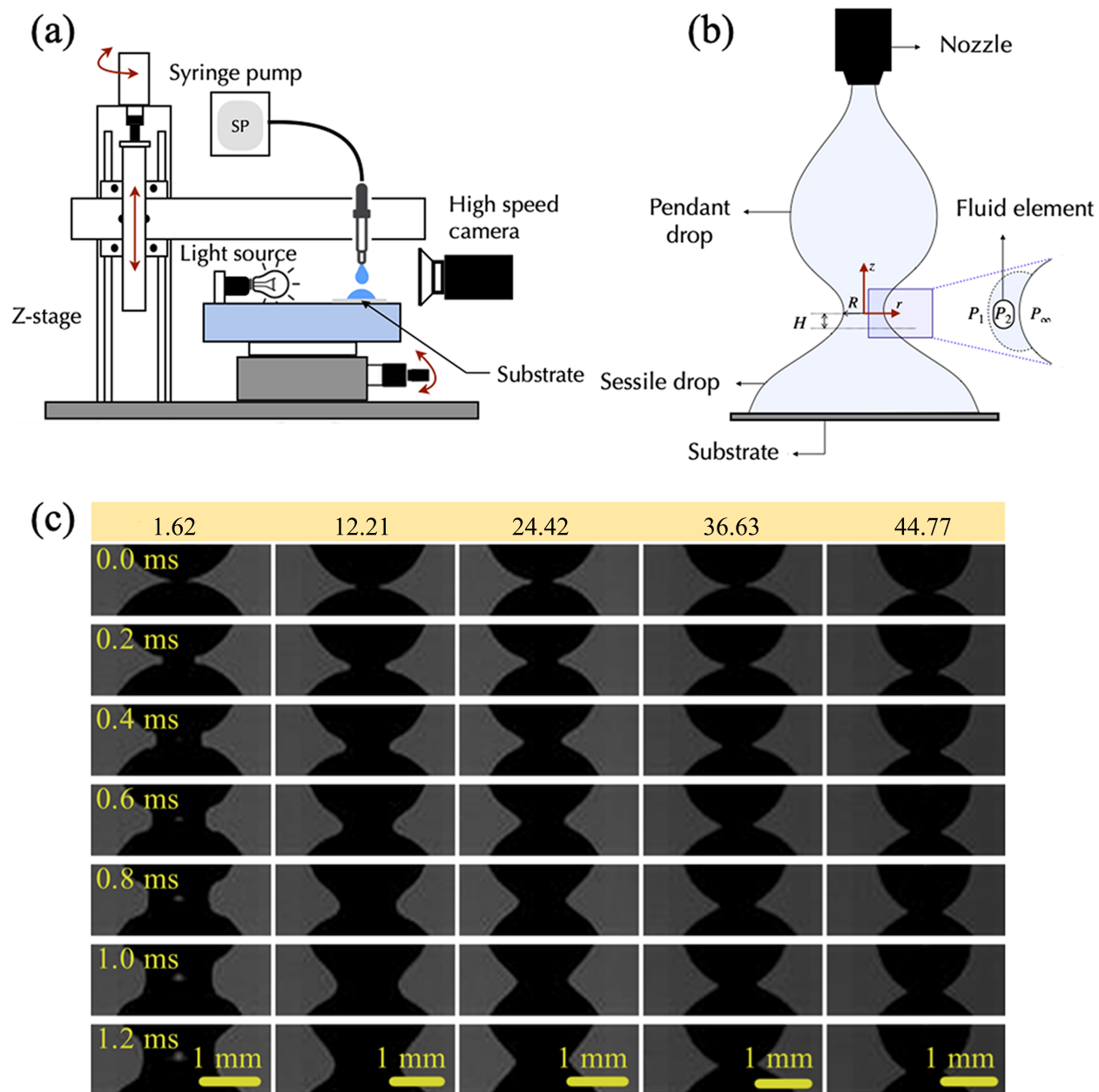


Figure 2: Schematics of (a) Experimental setup, (b) Neck region during coalescence representing the geometrical parameters during the process, (c) neck radius evolution of various concentration ratios: 1.63, 12.21, 24.42, 36.63, and 44.77 of PEO at different instants.

Results and Discussion

Coalescence proceeds via the formation of a liquid bridge during the merge of a pendant and sessile drop. This phenomenon is characterized by two geometric parameters namely the neck radius R and the neck semi-width H as shown in Fig. 2(b). The neck radius grows with time

due to the local curvature effects caused by surface tension σ . Such growth of neck radius for the concentration ratios: 1.63, 12.21, 24.42, 36.63, and 44.77 of PEO $M_w = 5 \times 10^6$ g/mol at different time instants are shown in Fig. 2(c). It is evident from Fig. 2(c) that for a particular time instant, the bridge curvature for different concentration ratios has a significant change as the ratio increases.

The temporal evolution of the neck radius, for various concentration ratios of the polymeric drops is shown in Fig. 3. The neck radius growth for the the concentration ratios represented in Fig. 3(a) are the averaged values of 5 trials. It can be seen that the bridge has slow growth initially followed by faster growth. As previously reported in the literature, it is seen that the neck growth follows the universal power-law growth function,¹⁴ $R = at^b$ which is equivalently the linear regime in Fig. 3. For different concentration ratios of polymeric droplets there is a decrease in neck speed due to the change in neck curvature. This is reflected in the power law index b . The variation of b for different concentration ratios of polymeric droplets is illustrated in Fig. 3(a). For $M_w = 5 \times 10^6$ g/mol, the value of b ranges from 0.38 to 0.16 while, for $M_w = 4 \times 10^6$ g/mol the value of b ranges from 0.39 to 0.25 for the range of concentration ratios explored in the current study. Fig. 3(b) shows the neck radius evolution of Polyethylene glycol (PEG) and Polyvinyl alcohol (PVA) obtained from Sarath et al.¹⁴ for $c/c^* < 1$ along with DI Water $c/c^* = 0$. It also shows the decrease in b from 0.5 to 0.4 with slight addition of Polymer in DI Water.

To encapsulate the coalescence dynamics in polymeric fluid droplets, it is crucial to outline the underlying forces. These underlying forces are, capillary force F_c , inertial force F_i , viscous force F_v , and elastic force F_e . Among these forces, F_c drives the bridge growth while the other three forces oppose it. The effect of these opposing forces F_i , F_v and F_e can be captured by three non-dimensional numbers: Reynolds number $Re = \langle \rho u_c l_c / \eta_o \rangle$, $Wi = \langle \lambda u_c / l_c \rangle$, and Elasticity number $El = \langle \eta_o \lambda / \rho l_c^2 \rangle$, where u_c and l_c represent characteristic velocity and length scales respectively, ρ is density, and η_o is zero shear viscosity. The characteristic scales associated with the flow are $u_c \sim \partial R / \partial t$ and $l_c \sim R$. The variation of these non-dimensional

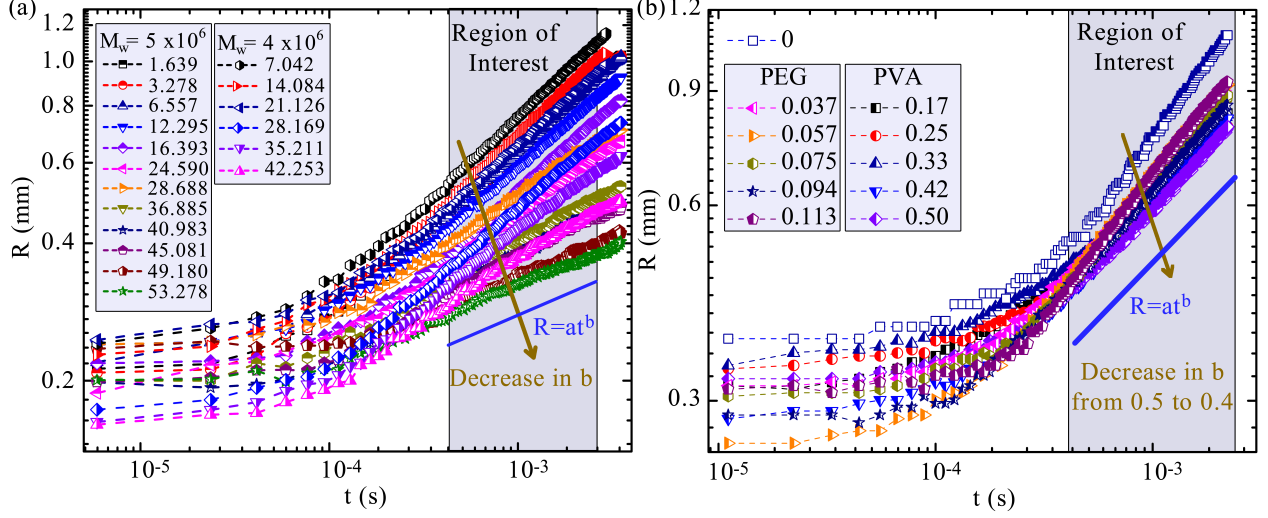


Figure 3: (a) Evolution of neck radius for various concentration ratios $c/c^* > 1$ of PEO solutions showing the decrease in intercept a and slope b with concentration ratios. (b) Neck radius evolution for $c/c^* < 1$ of Polyethylene glycol (PEG) and Polyvinyl alcohol (PVA) obtained from Sarath et al.¹⁴ along with DI Water ($c/c^* = 0$) representing the decrease in b from 0.5 to 0.4 with addition of polymer. (Note: The error in the measurements is less than 5%)

numbers with concentration ratio c/c^* is presented in Fig. 4. It reveals the presence of 3 regimes based on the concentration ratios. In the first regime, with concentration ratios $c/c^* < c_e/c^*$, the orders of corresponding numbers are $Re \sim \mathcal{O}(10)$, $Wi \sim \mathcal{O}(10^0)$ and $El \sim \mathcal{O}(10^{-1})$ suggesting the dominance of inertia force over viscous and elastic forces i.e. $F_i > F_v \approx F_e$. As the inertial forces are predominant, this regime is an inertio-elastic coalescence. While for the second regime, with the concentration ratios $c_e/c^* < c/c^* < c_c/c^*$ ($c_c/c^* \approx 20$), $Re \sim \mathcal{O}(10^{-1})$, $Wi \sim \mathcal{O}(10)$ and $El \sim \mathcal{O}(10^2)$ indicating that $F_e > F_v > F_i$. As the elastic forces are predominant followed by the viscous this regime is a viscoelastic coalescence. Similarly, for the regime with $c/c^* > c_c/c^*$, $Re < \mathcal{O}(10^{-1})$, $Wi > \mathcal{O}(10^2)$ and $El > \mathcal{O}(10^3)$ indicating that $F_e \gg F_v \gg F_i$. In this regime, the elastic forces are much greater than viscous forces, making it an elasticity dominant coalescence. Conclusively, as we increase the value of c/c^* , the coalescence phenomenon shifts from inertio-elastic to elasticity dominated regime.

The effect of the predominant forces in above 3 regimes are expounded by non-dimensionalizing,

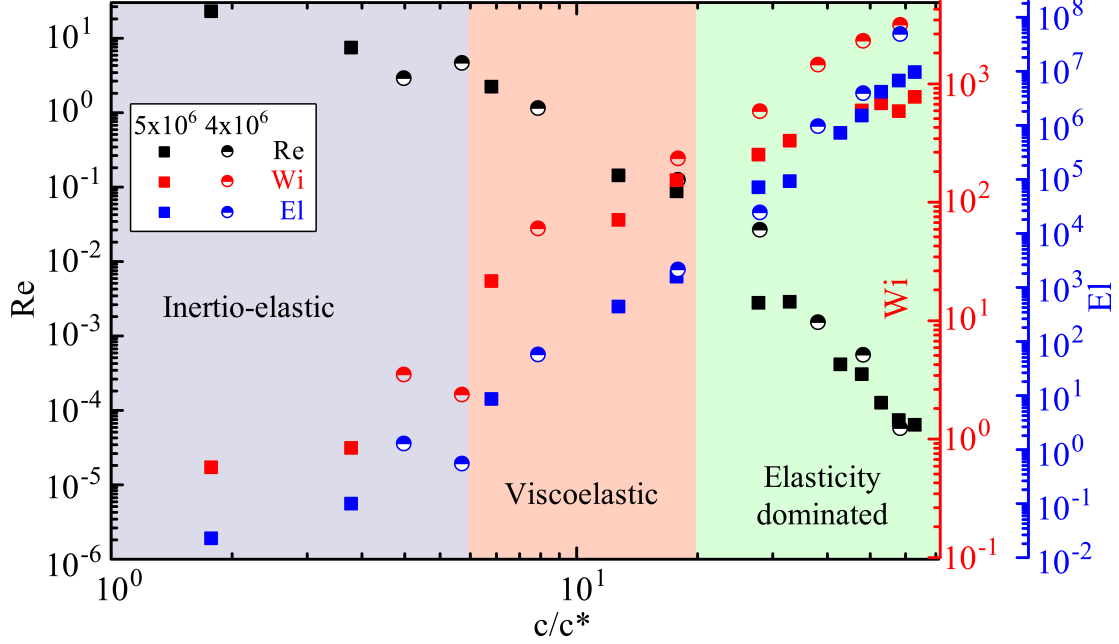


Figure 4: Comparison of predominant forces using Reynolds number, Weissenberg number, and Elastic forces representing the inertio-elastic, viscoelastic and elasticity dominated regimes with c/c^* for PEO of different molecular weights.

the radial r direction momentum equation under the quasi-radial assumption. The non-dimensional variables are defined as: $v_r^* = v_r/u_c$, $r^* = r/R$, $z^* = z/R$, $t^* = t/T$, $\tau_{rr}^* = \tau_{rr}/\tau_{RC}$, $\tau_{rz}^* = \tau_{rz}/\tau_{ZC}$, $p^* = p/P_c$, where $T := R/u_c$ and, $P_c := \sigma/R_o$ (R_o is the droplet radius) are the characteristic time and pressure respectively.

$$\frac{\rho u_c^2}{R} \left(\frac{\partial v_r^*}{\partial t^*} + v_r^* \frac{\partial v_r^*}{\partial r^*} \right) = -\frac{P_c}{R} \frac{\partial p^*}{\partial r^*} + \frac{\tau_{RC}}{R} \left(\frac{\tau_{rr}^*}{r^*} + \frac{\partial \tau_{rr}^*}{\partial r^*} \right) + \frac{\tau_{ZC}}{R} \frac{\partial \tau_{rz}^*}{\partial z^*} \quad (2)$$

The characteristic scales of stresses τ_{RC} and τ_{ZC} are obtained by introducing the previously defined non dimensional variables, along with the quasi-radial assumption in linear Phan Thien Tanner constitutive equation as follow:

$$\frac{\partial \tau_{rr}^*}{\partial t^*} + v_r^* \frac{\partial \tau_{rr}^*}{\partial r^*} - 2\tau_{rr}^* \frac{\partial v_r^*}{\partial r^*} + \frac{\tau_{rr}^*}{\frac{\lambda U}{R}} \left[1 + \frac{\kappa \lambda}{\eta} \tau_{RC} \tau_{rr}^* \right] = 2 \frac{\eta}{\lambda \tau_{RC}} \frac{\partial v_r^*}{\partial r^*} \quad (3)$$

$$\frac{\partial \tau_{rz}^*}{\partial t^*} + v_r^* \frac{\partial \tau_{rz}^*}{\partial r^*} - \tau_{rz}^* \frac{\partial v_r^*}{\partial r^*} + \frac{\tau_{rz}^*}{\frac{\lambda \bar{U}}{R}} \left[1 + \frac{\kappa \lambda}{\eta} \tau_{RC} \tau_{rr}^* \right] = \frac{\eta}{\lambda \tau_{ZC}} \frac{\partial v_r^*}{\partial z^*} \quad (4)$$

From eq (3) and eq(4) it is observed that the $\tau_{RC} := \eta/\lambda$, $\tau_{ZC} := \eta/\lambda$. By substituting these scales into eq (2), the dimensionless radial momentum equation is deduced as represented in eq(5).

$$\frac{\rho u_c^2 \lambda}{\eta} \left(\frac{\partial v_r^*}{\partial t^*} + v_r^* \frac{\partial v_r^*}{\partial r^*} \right) = -\frac{\sigma \lambda}{\eta R_o} \frac{\partial p^*}{\partial r^*} + \frac{\tau_{rr}^*}{r^*} + \frac{\partial \tau_{rr}^*}{\partial r^*} + \frac{\partial \tau_{rz}^*}{\partial z^*} \quad (5)$$

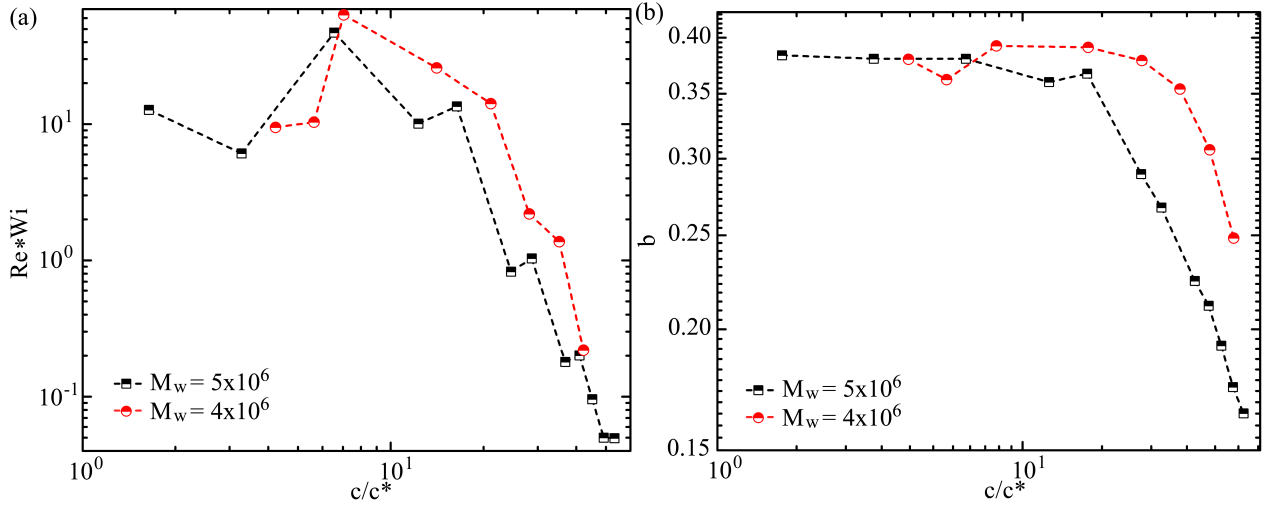


Figure 5: (a) Variation of $Re * Wi$ with c/c^* representing the decrease in $Re * Wi$ from $\mathcal{O}(10^1)$ to $< \mathcal{O}(10^0)$ from inertio-elastic/viscoelastic to elasticity dominated regime, (b) Representing the steady and monotonic decrease of b in inertio-elastic/viscoelastic regimes ($c/c^* < 20$) and elasticity dominated regime ($c/c^* > 20$) respectively.

The coefficient $\frac{\rho u_c^2 \lambda}{\eta}$, of inertial term in eq (5) is the product of Re and Wi , which is given as $Re * Wi = \langle \rho u_c^2 \lambda / \eta \rangle = \frac{\text{Elastic Force} \cdot \text{Inertia Force}}{(\text{Viscous Force})^2}$. The term $Re * Wi$ can be rewritten as $Re * Wi = \langle u_c^2 / U_s^2 \rangle$ where $U_s = \sqrt{\eta / \rho \lambda}$ ⁴³ is the shear wave velocity of the complex fluid. The values of $Re * Wi$ are presented for different concentration ratios in the Fig. 5(a). In the elasticity dominated regime, as observed in Fig. 4, the product of Re and Wi

is $Re * Wi = \langle u_c^2/U_s^2 \rangle \ll \mathcal{O}(10^0)$ while, for the other regimes $Re * Wi \sim \mathcal{O}(10^1)$. This implies that for the elasticity dominated regime, the characteristic velocity of the system u_c is less than the shear wave velocity of the fluid U_s while $u_c > U_s$ for the other regimes. The polymer chains begin to elongate along the shear direction after the droplets have touched each other. Such elongation decreases as the concentration of polymer increases due to polymer chain entanglements which alter the curvature of the liquid bridge, leading to the slow growth of the bridge and inhibiting the coalescence. In the elasticity dominated regime, the chains relax slower than the speed of information transfer hence the polymer chains are in unrelaxed state. On the contrary, for the other regimes, the polymer chains relax faster than the speed of information transfer implying that the chains have already relaxed to the external perturbation. This behaviour of chain relaxation leading to the decrease of exponent b in elasticity dominated regime where, $Re * Wi < \mathcal{O}(10^0)$ is represented in Fig. 5(b).

The effect of chain relaxation time is further demonstrated by considering the characteristic velocity u_c as the chain relaxation velocity, which can be defined as $u_c = R_o/\lambda$. On substitution, the term $\rho u_c^2 \lambda / \eta$ can be simplified as $\rho R_o^2 / \eta \lambda$. This simplified result can be rewritten as the ratio of time scales (τ^*) $\rho R_o^2 / \eta \lambda = t_c / \lambda = 1 / \tau^{*2}$ where, $t_c = t_i^2 / t_v$ is the Newtonian characteristic time. Here, $t_v = \eta R_o / \sigma$ is the viscous time scale and $t_i = \sqrt{\rho R_o^3 / \sigma}$ is the inertial time scale. It is observed from Fig. 6 that when $\tau^* < 10$, the exponent is constant with a value of 0.37 i.e the process is in inertio-elastic or viscoelastic regime. On contrary, when $\tau^* > 10$, the exponent decreases continuously. The dynamics governing the above phenomenon lies in the relaxing of polymer chains. When $\tau^* < 10$ the polymer chain relaxation are comparable to the Newtonian time scale t_c leading to a constant value. However, for $\tau^* > 10$, the polymer chains are in unrelaxed state even after the Newtonian time scale therefore altering the curvature of the bridge, resulting in the decline of b .

The universal behaviour of the neck radius evolution is proposed by Sarath et al.¹⁴ in inertio-elastic regime. To attain the universality Sarath et al.¹⁴ non dimensionalized the neck radius R using $\sqrt{\nu_o \lambda}$ as $R^* = R / \sqrt{\nu_o \lambda}$. Similarly, time t is non-dimensionalized with

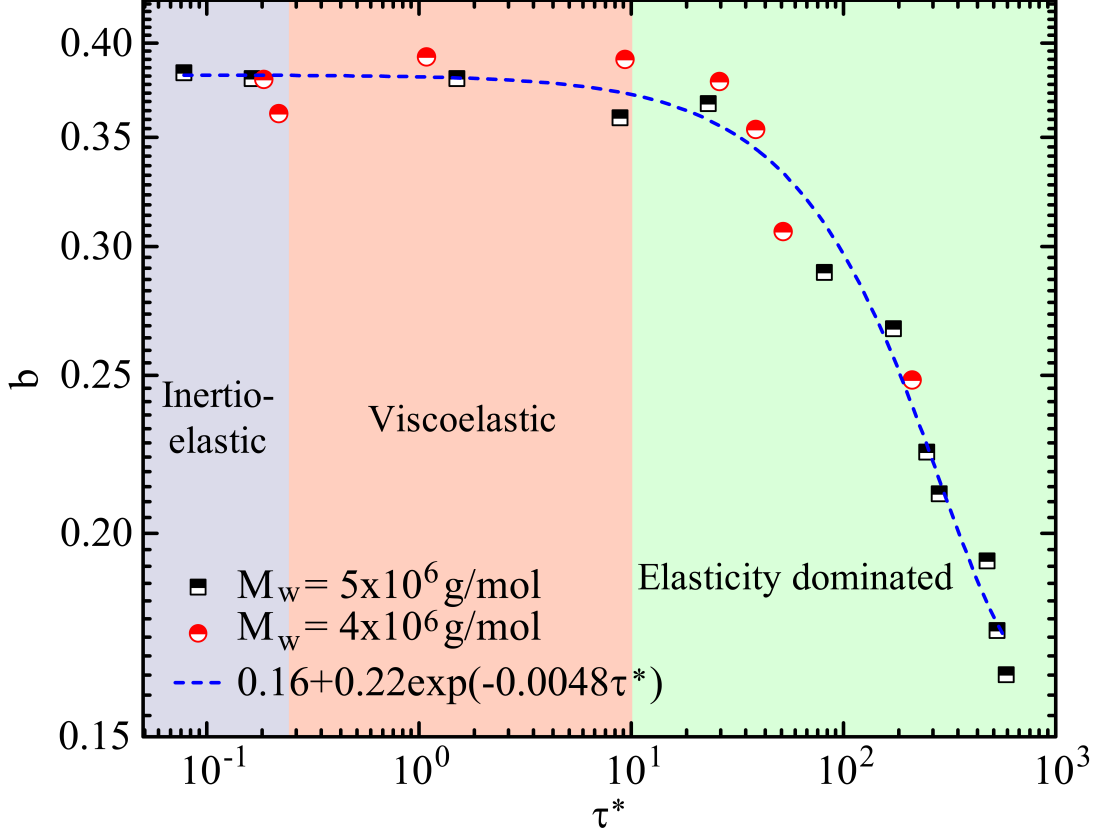


Figure 6: Dependence of the power law index b on the τ^* which is the ratio of relaxation time λ and Newtonian characteristic time t_c , with dashed blue line representing the exponential fit of 97% confidence interval for PEO solutions of different molecular weights.

$\lambda \text{Oh}^{-1} (\frac{c}{c^*})^{-1.2}$ leading to $t^* = (\frac{t}{\lambda} \text{Oh}^{-1}) (\frac{c}{c^*})^{-1.2}$. This non-dimensionalization led to the universal behaviour of the neck radius growth as $R^* \sim t^{*0.36}$ which is in agreement for the solutions in inertio-elastic and viscoelastic regimes having a constant value of $b = 0.37$ as represented in Fig. 6. However, such non-dimensionalization of neck growth breaks in the elasticity dominated regime. As the low Wi assumption is no longer valid, the previously reported governing equations is unable to capture the deviation from universality. This deviation shown in the inset of Fig. 7 is due to the incorrect characteristic length and time obtained from the balance of inertia, elastic and capillary forces, as the inertial forces are weak in the elasticity dominated regime. Moreover, in this regime, the polymer chains are not relaxed, hence the temporal variation of stress in the upper convected derivative should be considered, which was neglected in previous studies.¹⁴

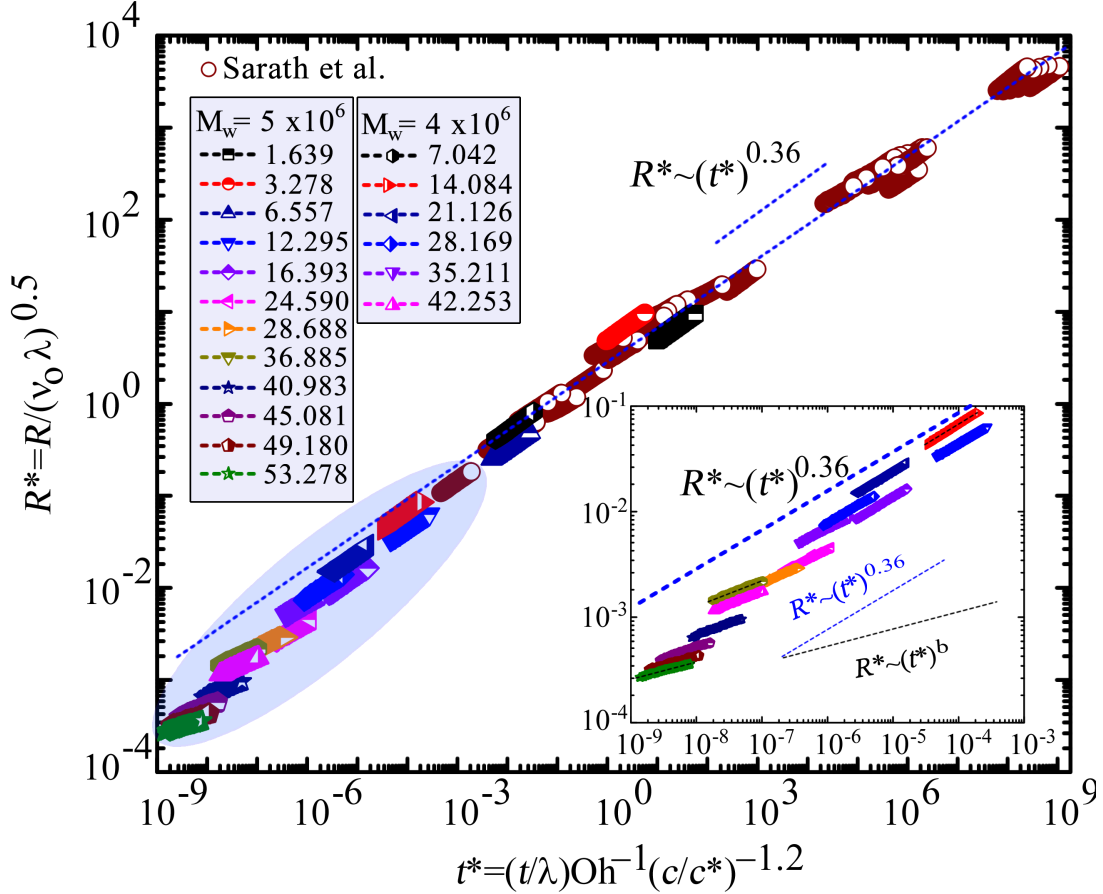


Figure 7: Non-dimensional neck radius as a function of non-dimensional time for all the polymer solutions used in this study and the previous study by Sarath et al.¹⁴ with legend representing corresponding c/c^* values. Inset shows the breaking of universality for $c/c^* > 10$ highlighted in the shaded region.

This deviation from universality in the elasticity dominated regime provides a novel method to determine the relaxation time λ of the complex fluids using the coalescence experiment. From Fig. 6 we propose a correlation between τ^* and b as $b = 0.16 + 0.22 \exp(-0.0048 \tau^*)$ for PEO. This correlation for PEO is validated by conducting coalescence experiments for concentration ratio $c/c^* = 32.56$ (2.0% w/v) of PEO $M_w = 5 \times 10^6$ solution having $\eta = 55$ Pa.s. Under similar experimental conditions, the temporal evolution of the neck for $c/c^* = 32.56$ is found to have the power-law exponent as $b = 0.275$. On substituting $b = 0.275$ in the correlation we obtain the relaxation time as $\lambda = 0.6$ s, which agrees with the relaxation time obtained from the SAOS experiments 1.35 s. Even though

there is a difference in the relaxation times, it is known that the relaxation time is method specific. For instance, the relaxation time obtained from the Capillary breakup extensional rheometer (CABER)⁴⁴⁻⁴⁷ and SAOS differ by an order.

In literature, many methods are proposed to measure the relaxation time of the fluid. Most widely used way to find λ is the linear viscoelastic response in a conventional rheometer.^{39,48} In this method, material is subjected to sinusoidal deformation to evaluate the viscous and elastic responses via loss modulus G'' and storage modulus G' respectively. The crossover of G' and G'' is used to determine the relaxation time of the fluid. But, this method is limited by the motor inertia in conventional rheometers and cannot capture the small values of λ . Hence for low relaxation times, a novel method named CABER, Capillary breakup extensional rheometer- Dripping on substrate (CABER-DOS)^{49,50} was proposed. However, the intrinsic difficulties in this method lies in the controlling of elongational flow. Such difficulties have led to the significant difference in relaxation times measured from the conventional method and by CABER. Recently, there are developments in microfluidic devices^{42,51,52} for overcoming the limitations of conventional rheometer and CABER, but, the fabrication of the microfluidic channel is intricate. However, the present study proposes a simple comprehensive tool named Rheocoalescence based on empirical correlations to determine the relaxation time of PEO solutions. Even though the proposed correlation can be used in all the regimes, it is robust in elasticity dominated regime. A comprehensive study on this method is required to generalize Rheocoalescence for all the polymeric fluids. The required experimental information for the correlation can be obtained easily, which makes this tool predominantly effective for cases where performing experiments by conventional methods become very difficult such as, the case of highly elastic fluid. This technique opens up a new paradigm in microfluidics and rheological measurements.

Conclusion

The current study demonstrates the effect of fluid elasticity on coalescence of pendant-sessile polymeric droplets. We performed high speed imaging to capture the temporal evolution of the bridge for a wide range of concentrations ratios. We reveal the presence of three regimes namely inertio-elastic, viscoelastic and elasticity dominated regimes based on c/c^* . The inertio-elastic regime occurs at $c/c^* < c_e/c^*$, and viscoelastic regime at $c_e/c^* < c/c^* < c_c/c^*$, similarly elasticity dominated regime at $c/c^* > c_c/c^*$. Experimentally, we have been able to demonstrate the dependence of power law index b on relaxation time leading to a novel method: Rheocoalescence to determine the relaxation time of the fluids. This opens a new paradigm in determining the characteristic time scales for wider class of complex fluids. However, the current study neglects the effect of surrounding fluid on the dynamics by considering air as the outer fluid. Further studies should be dedicated to extending this method's applicability for a variety of fluids along with the effect of outer fluid.

Acknowledgement

Supporting Information Available

References

- (1) Frenkel, J. Viscous flow of crystalline bodies under the action of surface tension. *J. phys.* **1945**, *9*, 385.
- (2) Eggers, J.; Lister, J. R.; Stone, H. A. Coalescence of liquid drops. *Journal of Fluid Mechanics* **1999**, *401*, 293–310.
- (3) Villiermaux, E.; Bossa, B. Single-drop fragmentation determines size distribution of raindrops. *Nature Physics* **2009**, *5*, 697.

- (4) Pruppacher, H. R.; Klett, J. D. *Microphysics of Clouds and Precipitation*; Springer, 2010; pp 10–73.
- (5) Ashgriz, N.; Poo, J. Coalescence and separation in binary collisions of liquid drops. *Journal of Fluid Mechanics* **1990**, *221*, 183–204.
- (6) Djohari, H.; Martínez-Herrera, J. I.; Derby, J. J. Transport mechanisms and densification during sintering: I. Viscous flow versus vacancy diffusion. *Chemical Engineering Science* **2009**, *64*, 3799–3809.
- (7) Orme, M. Experiments on droplet collisions, bounce, coalescence and disruption. *Progress in Energy and Combustion Science* **1997**, *23*, 65–79.
- (8) Rykaczewski, K.; Scott, J. H. J.; Rajauria, S.; Chinn, J.; Chinn, A. M.; Jones, W. Three dimensional aspects of droplet coalescence during dropwise condensation on superhydrophobic surfaces. *Soft Matter* **2011**, *7*, 8749–8752.
- (9) Barbosa, A. D.; Savage, D. B.; Siniosoglou, S. Lipid droplet–organelle interactions: emerging roles in lipid metabolism. *Current Opinion in Cell Biology* **2015**, *35*, 91–97.
- (10) Wilfling, F.; Haas, J. T.; Walther, T. C.; Farese Jr, R. V. Lipid droplet biogenesis. *Current Opinion in Cell Biology* **2014**, *29*, 39–45.
- (11) Paulsen, J. D.; Burton, J. C.; Nagel, S. R. Viscous to inertial crossover in liquid drop coalescence. *Physical Review Letters* **2011**, *106*, 114501.
- (12) Aarts, D. G.; Lekkerkerker, H. N.; Guo, H.; Wegdam, G. H.; Bonn, D. Hydrodynamics of droplet coalescence. *Physical Review Letters* **2005**, *95*, 164503.
- (13) Wu, M.; Cubaud, T.; Ho, C.-M. Scaling law in liquid drop coalescence driven by surface tension. *Physics of Fluids* **2004**, *16*, L51–L54.
- (14) Varma, S. C.; Saha, A.; Mukherjee, S.; Bandopadhyay, A.; Kumar, A.; Chakraborty, S. Universality in coalescence of polymeric fluids. *Soft Matter* **2020**,

- (15) Varma, S. C.; Saha, A.; Kumar, A. Coalescence of polymeric sessile drops on a partially wettable substrate. *Physics of Fluids* **2021**, *33*, 123101.
- (16) Ristenpart, W. D.; McCalla, P. M.; Roy, R. V.; Stone, H. A. Coalescence of Spreading Droplets on a Wettable Substrate. *Phys. Rev. Lett.* **2006**, *97*, 064501.
- (17) Lee, M. W.; Kang, D. K.; Yoon, S. S.; Yarin, A. L. Coalescence of two drops on partially wettable substrates. *Langmuir* **2012**, *28*, 3791–3798.
- (18) Case, S. C.; Nagel, S. R. Coalescence in low-viscosity liquids. *Physical Review Letters* **2008**, *100*, 084503.
- (19) Paulsen, J. D.; Burton, J. C.; Nagel, S. R.; Appathurai, S.; Harris, M. T.; Basaran, O. A. The inexorable resistance of inertia determines the initial regime of drop coalescence. *Proceedings of the National Academy of Sciences* **2012**, *109*, 6857–6861.
- (20) Blanchette, F.; Bigioni, T. P. Partial coalescence of drops at liquid interfaces. *Nature Physics* **2006**, *2*, 254.
- (21) Duchemin, L.; Eggers, J.; Josserand, C. Inviscid coalescence of drops. *Journal of Fluid Mechanics* **2003**, *487*, 167–178.
- (22) Hopper, R. W. Coalescence of two equal cylinders: exact results for creeping viscous plane flow driven by capillarity. *Journal of the American Ceramic Society* **1984**, *67*, C–262.
- (23) Hopper, R. W. Plane Stokes flow driven by capillarity on a free surface. *Journal of Fluid Mechanics* **1990**, *213*, 349–375.
- (24) Paulsen, J. D. Approach and coalescence of liquid drops in air. *Physical Review E* **2013**, *88*, 063010.
- (25) Paulsen, J. D.; Carmigniani, R.; Kannan, A.; Burton, J. C.; Nagel, S. R. Coalescence of bubbles and drops in an outer fluid. *Nature Communications* **2014**, *5*, 3182.

- (26) Ristenpart, W.; McCalla, P.; Roy, R.; Stone, H. A. Coalescence of spreading droplets on a wettable substrate. *Physical Review Letters* **2006**, *97*, 064501.
- (27) Yao, W.; Maris, H.; Pennington, P.; Seidel, G. Coalescence of viscous liquid drops. *Physical Review E* **2005**, *71*, 016309.
- (28) Decent, S.; Sharpe, G.; Shaw, A.; Suckling, P. The formation of a liquid bridge during the coalescence of drops. *International Journal of Multiphase Flow* **2006**, *32*, 717–738.
- (29) Gross, M.; Steinbach, I.; Raabe, D.; Varnik, F. Viscous coalescence of droplets: A lattice Boltzmann study. *Physics of Fluids* **2013**, *25*, 052101.
- (30) Sprittles, J.; Shikhmurzaev, Y. Coalescence of liquid drops: Different models versus experiment. *Physics of Fluids* **2012**, *24*, 122105.
- (31) Thoroddsen, S. T.; Takehara, K. The coalescence cascade of a drop. *Physics of Fluids* **2000**, *12*, 1265–1267.
- (32) Xia, X.; He, C.; Zhang, P. Universality in the viscous-to-inertial coalescence of liquid droplets. *Proceedings of the National Academy of Sciences* **2019**, *116*, 23467–23472.
- (33) Krebs, T.; Schroën, K.; Boom, R. Coalescence dynamics of surfactant-stabilized emulsions studied with microfluidics. *Soft Matter* **2012**, *8*, 10650–10657.
- (34) Vandebril, S.; Vermant, J.; Moldenaers, P. Efficiently suppressing coalescence in polymer blends using nanoparticles: role of interfacial rheology. *Soft Matter* **2010**, *6*, 3353–3362.
- (35) Thien, N. P.; Tanner, R. I. A new constitutive equation derived from network theory. *Journal of Non-Newtonian Fluid Mechanics* **1977**, *2*, 353–365.
- (36) Phan-Thien, N. A nonlinear network viscoelastic model. *Journal of Rheology* **1978**, *22*, 259–283.

- (37) Tirtaatmadja, V.; McKinley, G. H.; Cooper-White, J. J. Drop formation and breakup of low viscosity elastic fluids: Effects of molecular weight and concentration. *Physics of Fluids* **2006**, *18*, 043101.
- (38) Arnolds, O.; Buggisch, H.; Sachsenheimer, D.; Willenbacher, N. Capillary breakup extensional rheometry (CaBER) on semi-dilute and concentrated polyethyleneoxide (PEO) solutions. *Rheologica Acta* **2010**, *49*, 1207–1217.
- (39) Bird, R. B.; Armstrong, R. C.; Hassager, O. *Dynamics of polymeric liquids. Vol. 1, 2nd Ed. : Fluid mechanics*; Wiley, 1987.
- (40) Rubinstein, M.; Colby, R. H., et al. *Polymer physics*; Oxford University Press New York, 2003; Vol. 23.
- (41) Liu, Y.; Jun, Y.; Steinberg, V. Concentration dependence of the longest relaxation times of dilute and semi-dilute polymer solutions. *Journal of Rheology* **2009**, *53*, 1069–1085.
- (42) Del Giudice, F.; D’Avino, G.; Greco, F.; De Santo, I.; Netti, P. A.; Maffettone, P. L. Rheometry-on-a-chip: measuring the relaxation time of a viscoelastic liquid through particle migration in microchannel flows. *Lab on a Chip* **2015**, *15*, 783–792.
- (43) Joshi, P.; Shankar, V. Flow-induced resonant shear-wave instability between a viscoelastic fluid and an elastic solid. *Physics of Fluids* **2019**, *31*, 084107.
- (44) Zell, A.; Gier, S.; Rafai, S.; Wagner, C. Is there a relation between the relaxation time measured in CaBER experiments and the first normal stress coefficient? *Journal of non-newtonian fluid mechanics* **2010**, *165*, 1265–1274.
- (45) Tirtaatmadja, V.; McKinley, G. H.; Cooper-White, J. J. Drop formation and breakup of low viscosity elastic fluids: Effects of molecular weight and concentration. *Physics of fluids* **2006**, *18*, 043101.

- (46) Meissner, J.; Hostettler, J. A new elongational rheometer for polymer melts and other highly viscoelastic liquids. *Rheologica Acta* **1994**, *33*, 1–21.
- (47) Pathak, J. A.; Hudson, S. D. Rheo-optics of equilibrium polymer solutions: Wormlike micelles in elongational flow in a microfluidic cross-slot. *Macromolecules* **2006**, *39*, 8782–8792.
- (48) Larson, R. G. *The structure and rheology of complex fluids*; Oxford university press New York, 1999; Vol. 150.
- (49) Jimenez, L. N.; Dinic, J.; Parsi, N.; Sharma, V. Extensional relaxation time, pinch-off dynamics, and printability of semidilute polyelectrolyte solutions. *Macromolecules* **2018**, *51*, 5191–5208.
- (50) Dinic, J.; Zhang, Y.; Jimenez, L. N.; Sharma, V. Extensional relaxation times of dilute, aqueous polymer solutions. *ACS Macro Letters* **2015**, *4*, 804–808.
- (51) Pipe, C. J.; McKinley, G. H. Microfluidic rheometry. *Mechanics research communications* **2009**, *36*, 110–120.
- (52) Zilz, J.; Schäfer, C.; Wagner, C.; Poole, R. J.; Alves, M. A.; Lindner, A. Serpentine channels: micro-rheometers for fluid relaxation times. *Lab on a Chip* **2014**, *14*, 351–358.